ELSEVIER

Contents lists available at ScienceDirect

Materials Science & Engineering A

journal homepage: http://www.elsevier.com/locate/msea





Size-temperature equivalence in tensile deformation of metallic glass

Chandra Sekhar Meduri ^a, Jerzy Blawzdziewicz ^b, Golden Kumar ^{a,*}

- ^a Department of Mechanical Engineering, The University of Texas at Dallas, Richardson, TX, 75080, USA
- b Department of Mechanical Engineering, Texas Tech University, Lubbock, TX, 79409, USA

ABSTRACT

Tensile fracture of irradiation-free metallic glass specimens with diameters ranging from 100 nm to $500 \text{ }\mu\text{m}$ is investigated at different temperatures. A gradual change in fracture morphology from vein-pattern to completely smooth fracture surface to necking is observed with decreasing sample size and testing temperature. The size-temperature equivalence in the entire length scale can be described by considering the thermal effects in shear localization of metallic glasses. We construct an empirical model based on the shear band heating and velocity formulations to qualitatively describe the size and temperature effects on the fracture morphology. Our results suggest that the widely reported size-dependent transition from shear-localized to homogeneous flow in metallic glasses is fundamentally different from the high temperature homogeneous viscous flow. The plastic deformation in nanoscale samples is spatially localized in embryonic shear bands, which never mature to the propagation stage due to lack of heat content.

1. Introduction

Size-effects in deformation behavior of metallic glasses (MGs) have gained increasing interest due to their potential in overcoming the intrinsic weakness of shear localization. Room temperature plastic deformation in macroscopic MGs is localized in thin shear bands that limit the overall plasticity [1-6]. Multiple shear bands can form under constrained loadings to accommodate some plastic strain, but a single shear band becomes an unstable crack under tension [7-10]. In contrast, sub-micron sized samples of different MGs have been reported to deform homogeneously with substantial necking and tensile ductility [11-14]. Numerous experimental and simulation studies have been focused on small-scale samples but the existence and the mechanism of size-dependent change in deformation mode in MGs remain unsettled [15–20]. Many researchers have reported homogeneous-like necking in tensile [11,13,14] and bulging in compression [21–25] when the sample diameter is reduced below 500-600 nm but others observed no such change with decreasing sample size [26,27].

The contradicting observations in size-effects of MGs stem from multiple factors such as, improper sample geometry, the use of high-energy irradiation in sample preparation, variation in glassy state with sample size, and limited statistics of *in-situ* nanomechanical tests. It has been shown that inherent tapering in nanoscale pillars machined by focused-ion-beam (FIB) can alter the stress state and complicate the interpretation of true size-effects [27,28]. However, Kuzmin et al. demonstrated that even taper-free MG samples exhibit change in deformation mode with decreasing sample size [29]. Magognosc et al.

correlated the size-effects to FIB irradiation and reported inhomogeneous flow in non-irradiated MGs with diameters down to 150 nm [30, 31]. Yi et al. decoupled the irradiation effects by testing the MG nanofibers directly drawn from the liquid state and showed that change in deformation mode at nanoscale is an intrinsic feature of MGs [13].

The origin of size dependence in plastic deformation of MGs has also been controversial. Volkert et al. and others used the stored elastic energy versus shear band energy crossover criterion to explain the absence of shear bands in smaller samples [11,14,21]. Yi et al. argued that the departure from shear banding is observed because the sample diameter becomes comparable to the critical size of shear band nucleus, which was estimated to be about 500 nm [13]. Recently, Tonnies et al. showed that the size-dependent deformation mode of MGs is strongly affected by the loading rate [32]. They argued based on the concept of shear band spacing that the "seemingly" homogeneous flow observed in nanoscale samples can be envisioned as the entire volume deforming in shear bands. Similar hypothesis was advanced earlier by Schuh et al. based on the nanoindentation results where the non-serrated flow observed at high loading rates or low temperatures was labeled as "homogeneous II" to distinguish it from the homogeneous viscous flow of MGs [33]. It remains unclear if the size-dependent homogeneous flow in MGs is like the viscous flow consisting of uncorrelated shear-transformation-zones (STZs) or homogeneous II-type flow consisting of non-propagating embryonic shear bands.

Observation of vein-pattern and liquid droplets on the fracture surface indicate large temperature increase during plastic deformation and failure of MGs. Effect of temperature rise in shear bands has been

E-mail address: golden.kumar@utdallas.edu (G. Kumar).

^{*} Corresponding author.

extensively investigated by computer simulations and thermal imaging techniques [34–39]. While the reported values of temperature vary widely in different studies, heating is not considered as the cause of shear localization in MGs. However, recent *in-situ* thermal imaging studies show a strong correlation between the different stages of shear banding and temperature spikes [40]. Thermal effects have been analyzed in the context of size-effects to explain the catastrophic failure in thick (>1 mm) MGs [38,41]. However, the role of heating in nanoscale size-effects remains unexplored due to challenging spatial requirements.

The size-effects in MGs are typically investigated in two distinct regimes i.e., sub-micron and above 1 mm [11,18,21–23,42], which leaves a large uncharted size range that can provide an important information about the underlying mechanism. Here, we address the existing issues by studying tensile specimens of MG with diameters ranging from 100 nm to 500 μ m. Use of tensile loading ensures uniaxial stress in nanoscale specimens unlike compression testing of tapered columns. The samples were produced by thermoplastic drawing to eliminate the irradiation artifacts. Arrays of samples with varying diameters were simultaneously fabricated from the same piece of MG to minimize the variation in glassy state and yield statistically reliable data. Multiple samples of each diameter were fractured in tension at different temperatures to understand the mechanism of size-dependent deformation mode.

2. Experimental

Pt₅₇₋₅Cu₁₄₋₇Ni₅₋₃P_{22.5} (Pt-based) ingot was prepared by melting highpurity elements in a vacuum-sealed quartz tube. The ingot was melted and fluxed with B₂O₃ to improve the glass forming ability. A cylindrical MG sample with a diameter of 2 mm was produced by water quenching the molten alloy in a thin-wall quartz tube. Amorphous state of quenched samples was verified using x-ray diffraction and differential scanning calorimeter. Irradiation-free tensile specimens were prepared by thermoplastic drawing illustrated in Fig. 1. Lithographically fabricated silicon and machined aluminum were used as molds for drawing arrays of MG specimens. The molds were secured to a heating plate installed on the lower compression plate of Instron mechanical tester. The MG disc was anchored to the top heating plate using steel mesh and custom-made fixtures. The MG disc was pressed and pulled against the molds heated above the glass transition temperature ($T_g = 503$ K). As reported previously, thermoplastic press-and-pull technique can produce MG fibers with sub-micron diameters [43-45]. In this study, samples with diameters (D) of 100 nm-500 µm were drawn by using cylindrical mold cavities with diameters in the range of 10 μm to 1 mm.

The drawn samples were equilibrated at the desired testing temperature below T_g before tensile loading. The short thermal conditioning is not expected to affect the deformation mode because the Pt-based MG is resistant to thermal embrittlement during sub- T_g relaxation [46]. The

elongation rate was selected to yield the initial strain-rate in the range 10^{-3} - 10^{-1} s⁻¹, where shear banding is the dominant deformation mode in bulk samples below $T_{\rm g}$. The highest testing temperature was limited to 433 K to prevent interference with the viscous flow which can exist well below the calorimetric $T_{\rm g}$ in MGs. About 20–30 samples for each D were fractured and characterized by scanning electron microscope (SEM). The representative SEM images (Fig. 1) demonstrate the feasibility of proposed methodology for characterization of size-dependent deformation mode in MGs. The fracture surface was analyzed in the case of shear-localized specimens and the change in diameter along the neck was measured for the necked specimens.

3. Results

Fig. 2 shows the SEM images of Pt-based MG samples fractured at room temperature $(0.6T_g)$. A clear transition from shear-localized failure to necking is observed when the sample diameter reduces below 500 nm. The size range for observed transition is consistent with previous work on irradiation-free Pd-based MG nanofibers [13]. All the shear-localized specimens fractured at an angle of about 55° with the loading direction irrespective of sample size, which is a characteristic feature of MGs failed along dominant shear band in tension [3,8–10,47]. The fracture surface of shear-localized samples consists of two distinct regions i.e., smooth area and vein-pattern (separated by dashed line in Fig. 2). As shown by the inset image for 500 µm diameter sample, the veins appear to radiate from the center of featureless cores. However, the core-like morphology was not observed in samples with diameters smaller than 70 µm but interconnecting veins and dimples were still evident. The fracture morphology changes to fewer veins and eventually to a single branching central vein for diameters smaller than 20 µm. Along with these changes in the vein-pattern, the fraction of smooth area continues to rise with decreasing sample diameter. The samples with diameters in the range of 2 μ m-500 nm displayed only smooth fracture surfaces. The fracture deviated from 55° plane to diffuse morphology for 400 nm diameter sample, marking the departure from single dominant shear band. Smaller samples exhibited profuse necking and the neck length increased with decreasing sample diameter. Similar trend in size-dependent fracture morphology was observed at other testing temperatures but the changes in fractographic features occurred at different diameters with varying temperature. The variations in fracture morphology were quantified to understand the correlation between the sample-size, the testing temperature, and the deformation mode.

The smooth region on the fracture surface corresponds to slip of a shear band and the presence of vein-pattern indicates the formation of liquid-like layer due to heating [4]. The tensile loading results in cavitation and catastrophic failure when the liquid layer of sufficiently low viscosity forms. The slip (δ_S) was measured as the projection of shear-offset in the plane perpendicular to the loading axis as shown in

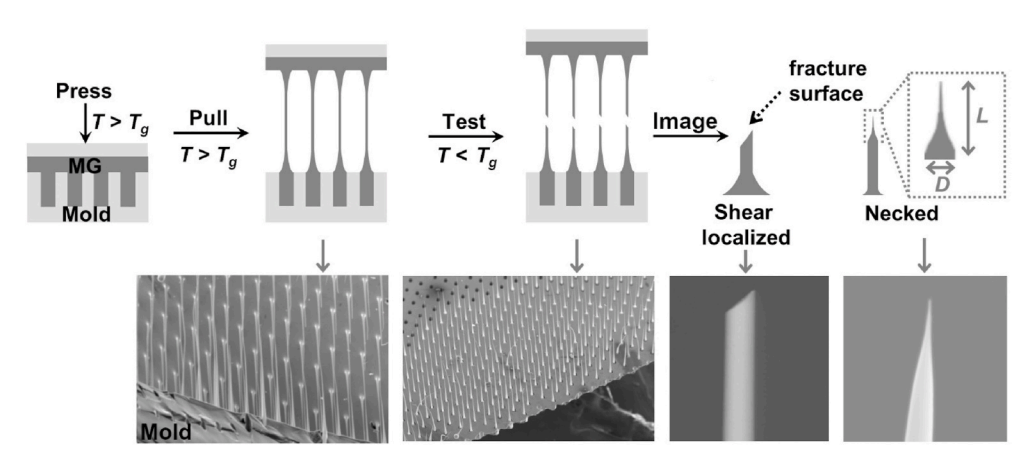


Fig. 1. Schematic illustration of fabrication and testing of MG tensile specimens. Multiple samples with varying diameters are fabricated by thermoplastic ($T > T_g$) pressand pull technique using different molds. The drawn samples are cooled below T_g and fractured in tension at different temperatures followed by imaging analysis. Two fracture morphologies (shear-localized and necked) are observed depending on the combination of sample diameter and testing temperature. The SEM images show examples of sample array before and after fracture, and the closer views of shear-localized and necked geometries using Pt-based MG.

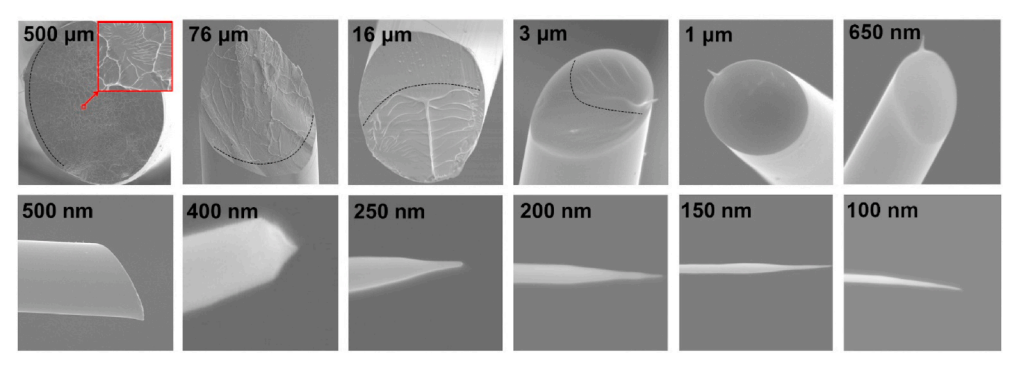
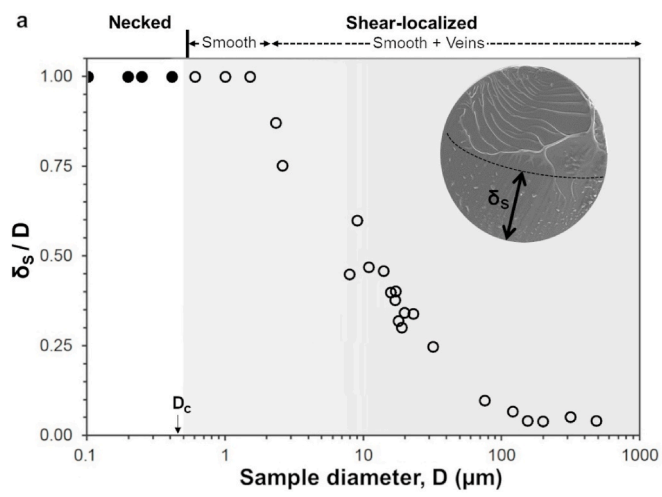


Fig. 2. SEM images of Pt-based MG tensile samples fractured at 298 K. The sample diameters are mentioned in the upper-left corner of each image. The samples with diameters larger than 450 nm fractured along a localized shear band while necking is observed for smaller diameters. The fracture surface of shear-localized samples consists of smooth and vein-pattern regions (separated by dash line) whose fractions vary with sample diameter. The inset of 500 μm diameter sample shows veins radiating from central cores which were observed on the fracture surface of all samples with diameters larger than 70 µm. A featureless fracture surface is observed in the range of 500 nm to 2 µm diameter samples. In the necked samples, the neck length becomes longer with decreasing increasingly diameter.

the inset of Fig. 3a. At room temperature, the δ_S/D remains less than 5% for large samples (D=70–500 µm) but increases rapidly for D<70 µm



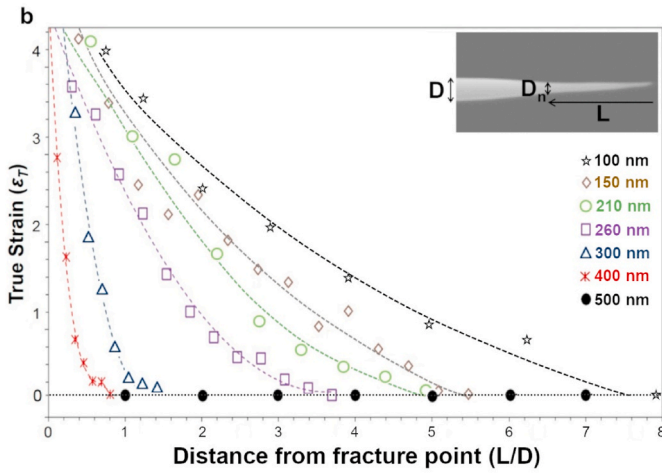


Fig. 3. Quantitative analysis of Pt-based MG samples fractured at 298 K. (a) Normalized shear-offset (δ_S/D) as a function of sample diameter (D) for the shear-localized samples. The inset SEM image shows typical δ_S projected on a plane perpendicular to the loading axis. Necking is observed below critical diameter $D_c{\sim}450$ nm (filled symbols). (b) True strain $(\varepsilon_T=\ln(D^2/D_n^2))$ vs normalized distance from the fracture point (L/D) for the necked samples. The inset SEM image illustrates different parameters used in calculation of ε_T . The shear-localized sample of 500 nm diameter is also shown for comparison.

before saturating to 100% for $D\sim 2$ –3 µm (Fig. 3a). A large δ_S/D indicates stable shear band propagation before developing a liquid layer. Therefore, the shear band stability increases with reduction in sample diameter. At $D\sim 2$ µm, formation of the vein-pattern is completely averted, and the MG fails by pure shear resulting in smooth fracture surface.

With further decrease in D (till \sim 500 nm), the fracture surface remains free of veins, but failure still occurs along a single dominant shear band inclined at 55°. A transition from single shear band to distributed flow was observed at critical diameter $D_c \sim 450$ nm, and profuse necking was observed in samples with D lower than 400 nm (filled symbols in Fig. 3a). To quantify the necking effect, true strain values ($\varepsilon_T = \ln (D^2/D^2)$ (L/D) at different normalized distances (L/D) from the fracture site were measured following the procedure described by Yi et al. [13]. Where D is the initial sample diameter and D_n is the diameter in the necked region at a distance L from the point of fracture. Fig. 3b shows the corresponding ε_T plot for samples failed by necking at room temperature. A shear-localized sample (D = 500 nm) is also shown for reference for which ε_T remains zero because of absence of necking. However, the necked samples show increasing neck length with decreasing sample diameter. The neck length increased from 0.9D for 400 nm sample to 8D for 100 nm sample.

The fractographic features were quantified at different testing temperatures in the range 200 K–433 K (0.4 T_g -0.8 T_g). Fig. 4a compares the δ_S/D as a function of sample diameter for three testing temperatures. It is evident that the testing temperature has negligible effect on δ_S/D for $D \geq 70~\mu m$. All these large samples showed veins emerging from central cores on the fracture surface and δ_S/D remained less than 10%. However, the testing temperature significantly affects the fracture morphology for $D < 70~\mu m$. The δ_S/D increases with decreasing testing temperature for a fixed D. The effect can be clearly seen in the SEM images of 10 μ m diameter samples fractured at different temperatures (Fig. 4b).

The fraction of smooth region increases at the expense of vein-pattern with decreasing temperature. The testing temperature has an equivalent effect as the sample diameter on δ_S/D . The transition from vein-pattern to smooth fracture surface shifts to larger diameters with decreasing testing temperature. The transition is observed at diameter of 300 nm at 433 K and it shifts to 5 μ m at 200 K. Interestingly, the transition from shear-localized to necking also shows the same trend with varying temperature. As shown in Fig. 4c, a 300 nm diameter specimen failed by shear localization at 433 K, but showed necking at 298 K. At 433 K, the necking was only observed for diameter of 210 nm or smaller (Fig. 4c). Therefore, decrease in testing temperature and sample diameter facilitate suppression of vein-pattern and severe localization.

The effect of testing temperature on the true strain was also analyzed

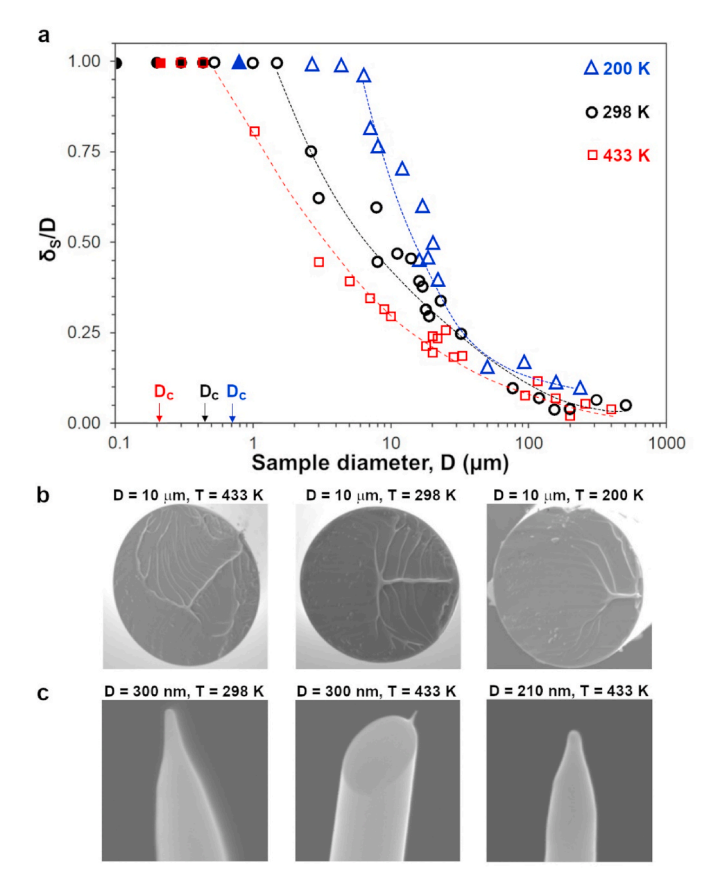


Fig. 4. Effect of testing temperature on the fracture behavior. (a) The comparison of δ_S/D vs D plots for samples tested at 200 K (0.4 T_g), 298 K (0.6 T_g), and 433 K (0.8 T_g). The open and filled symbols are for shear-localized and necked samples, respectively. (b) Fracture surfaces of 10 μ m diameter samples tested at three different temperatures. (c) Side views of 300 nm diameter sample necked at 298 K, 300 nm diameter sample shear-localized at 433 K, and 210 nm diameter sample necked at 433 K.

in the necked samples. The true strain plots for $D\sim150$ nm samples fractured at different temperatures are shown in Fig. 5. The maximum neck length increased from $\sim\!2D$ at 433 K to $\sim\!5.5D$ at 298 K. The necking of 150 nm diameter sample at 433 K (0.8 T_g) is not due to approaching the supercooled liquid state because the samples with larger diameters failed by shear localization at 433 K. The structural

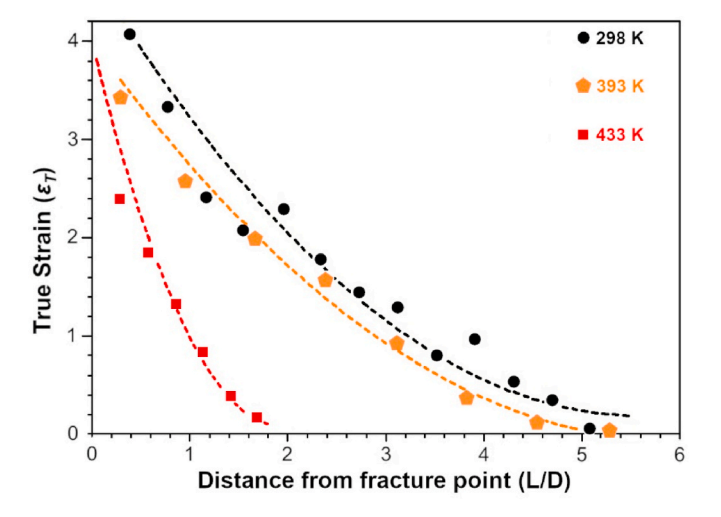


Fig. 5. Effect of temperature on necking. True strain vs L/D plots for 150 nm diameter samples necked and fractured at different temperatures.

relaxation induced embrittlement can also be disregarded because the estimated relaxation time for Pt-based MG at 433 K is longer about $10^{12}\,\mathrm{s}$ [46]. By comparing the results of temperature (Fig. 5) and size (Fig. 3b) dependent true strain, one can clearly see that a decrease in sample diameter and testing temperature enhances the tensile ductility in nanoscale MGs. These observations indicate that the size-temperature equivalence in tensile fracture of MGs persists over the entire range of sample diameters.

It is worth noting that the size-dependent necking in MGs is different from the high temperature homogeneous viscous flow. Ductility associated with viscous flow typically increases with temperature in MGs whereas the size induced ductility exhibits an opposite trend (Fig. 5). The effect of sample size on ductility is also contrary in two homogeneous regimes. The neck length shortens with decreasing sample diameter in viscous state due to increasing capillary stress [45], however the neck length increases with decreasing sample diameter at room temperature (Fig. 3b). Furthermore, the global ductility due to room temperature is limited 5–30% suggesting that high stress sensitivity probably persists in nanoscale samples. In contrast, elongation exceeding 200% has been routinely achieved in viscous state of MG. These disparities indicate that the physical origin of homogeneous-like flow well below T_g and true homogeneous viscous flow in MGs is different.

4. Discussion

To understand the correlation between the sample size and the testing temperature, we refer to the two-stage model [4,40,48] for shear band formation in MGs (Fig. 6). In stage I, plastic deformation begins by rearrangement cluster of atoms referred shear-transformation-zones (STZs). Multiple STZs can nucleate at stress concentration sites or structural heterogeneities when the shear stress exceeds the critical value. Formation of an STZ results in localized strain-softening and subsequent STZs are accumulated in the vicinity, forming an embryonic shear band (ESB). The growth of an ESB occurs by progressive shear front at velocity approaching the transverse sound wave ($\sim 10^3$ m/s). It is widely accepted that STZ to ESB transition is caused by structural softening without significant heating because the overall amount of plastic work is small [2,49,50]. At this stage, the competition between multiple ESBs initiated at different STZ sites can exist. One of the ESBs exceeds the critical length (lc) and becomes a mature shear band (MSB) accelerating across the sample at increasing strain-rate compared to the rest of the glass. The transition from ESB to MSB is the key in understanding the apparent size-dependent change in deformation mode of MGs. Once an MSB nucleates, any subsequent plastic strain is accommodated by the cooperative sliding across the weakened band as depicted in stage II (Fig. 6). An MSB subjected to tensile stress becomes unstable mode-I crack due to increasing cavitation resulting in zero global ductility. Under constrained loading such as compression, an MSB can exhibit stick-slip motion depending on the testing temperature and the applied strain-rate [40,51-53]. In the following, we first discuss the effects of sample size and testing temperature on the fracture surface of shear-localized samples using the stage II shear band dynamics. Subsequently, we analyze the transition from shear localization to necking in nanoscale samples and its correlation with the nucleation of an MSB.

The catastrophic failure of large MG samples is caused by the instability of liquid layer formed due to heat generated during the sliding of MSB (stage II in Fig. 6). On the fracture surface, the smooth region corresponds to the initial sliding of MSB and the vein-pattern is an indicator of subsequent Saffman-Taylor instability in the liquid layer [4]. We consider δ_S as the projection of shear-offset at which liquid layer reaches critical viscosity (or equivalently temperature) and dimensions to initiate the instability. Our results show that the sample diameter and the testing temperature have similar effect on δ_S (Fig. 4a). This size-temperature equivalence can be understood by analyzing the

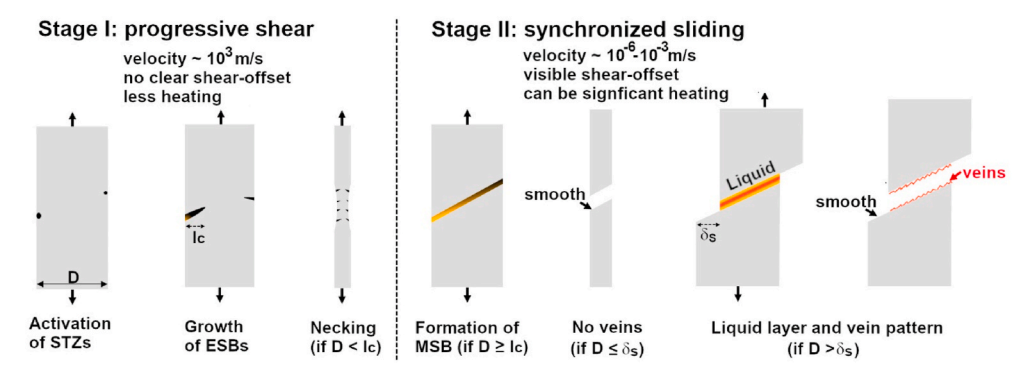


Fig. 6. Two-stage model for formation of shear band in MG under tension. In stage I, STZs nucleate and localize into embryonic shear bands (ESBs) by moving the shear front at high velocity. The samples with diameters smaller than the critical length (l_c) deform through multiple ESBs whilst a mature shear band (MSB) nucleates in the samples with larger diameters. In stage II, deformation proceeds by synchronized sliding of two sample pieces across the MSB. If the sample diameter is smaller than δ_{S_1} smooth fracture surfaces are formed because of insufficient heating. For samples with diameters larger than δ_S , a liquid layer forms and results in different vein morphologies upon rupture.

competing timescales: shear time (t_S) and the time to attain viable liquid layer (t_L) . The heat is generated over time t_S in thin MSB and it takes finite time t_L to form liquid layer because of thermal diffusion from the MSB to the bulk material. The t_S can be expressed as:

$$ts = \frac{\delta}{V_{\rm c}} \tag{1}$$

where V_S is the sliding velocity of MSB to create shear-offset δ . There has been a significant uncertainty in the values of V_S reported in literature. In earlier studies, V_S was assumed to be close to the velocity of transverse sound wave [37]. In contrast, longer shear times calculated from the stress-strain data suggest that the maximum value of V_S should be an order of magnitude smaller [54,55]. Recently, Maass et al. measured even lower values of $V_S \sim 10^{-6} \cdot 10^{-2}$ m/s and observed a strong temperature dependence [52]. These studies, however, did not consider the effect of sample size on V_S while it is evident that the driving force for shear band propagation should also be a function of sample size. According to continuum mechanics, a crack attains increasingly higher velocity with increasing elastic energy release rate in brittle materials [56]. By treating the shear band as a mode II crack, similar energy-based approach can be used to express V_S :

$$V_S = V_o \left(1 - \frac{E_{SB}}{E_{EL}} \right) \tag{2}$$

where V_o is the maximum shear band velocity which should be a function of temperature and applied strain-rate, E_{SB} is the shear band energy, and E_{EL} is the stored elastic energy. The E_{SB} is a combination of structural disorder energy generated by shearing and the surface energy due to shear-offset. The exact value of E_{SB} is debatable but it does not change the outcome of following discussion. Eq. (2) is valid only in stage II when there is surplus energy supply ($E_{EL} > E_{SB}$) to drive the propagation of MSB. It can be rewritten in terms of sample diameter as:

$$V_S = V_o \left(1 - \frac{e_{SB} D^2}{e_{EL} D^3} \right) = V_o \left(1 - \frac{D_c}{D} \right) \tag{3}$$

where e_{SB} has units of energy per unit area and e_{EL} has units of energy per unit volume. The ratio e_{SB}/e_{EL} has units of diameter which can be envisioned as the critical diameter D_c below which shear band propagation is energetically not favorable. Therefore, Eq. (3) is valid only for $D > D_c$ while $D \le D_c$ falls in the necking regime that will be discussed later. Eq. (3) predicts increase in V_S with increasing sample diameter, which is in qualitative agreement with previous findings [19,38]. By substituting the value of V_S , Eq. (1) takes the form:

$$ts = \frac{\delta}{V_o(1 - D_c/D)} \tag{4}$$

Miracle et al. investigated the thermal profiles around a propagating shear band by treating it as a planar source of heat [41]. The time for which the hot zone heated above a reference temperature T_R reaches the maximum width was calculated as:

$$t = Z \left(\frac{\delta}{T_P - T}\right)^2 \tag{5}$$

where T is the environmental temperature and Z combines the numeric constants and the material properties such as, thermal diffusivity, volumetric specific heat, and shear stress of shear band [41]. Assuming the MSB becomes prone to instability when the associated hot zone reaches the liquidus temperature (T_L), the corresponding time t_L can be calculated from Eq. (5):

$$t_L = Z \left(\frac{\delta}{T_I - T}\right)^2 \tag{6}$$

The choice of liquidus or glass transition temperature for liquid layer instability only affects the absolute value of t_L but its temperature dependence remains unchanged. The liquid layer will develop if the heat is generated faster than it is diffused away from the MSB. Therefore, $t_S \leq t_L$ is the required condition for observation of vein-pattern on the fracture surface of MGs. Both t_S and t_L rise with increasing δ , and failure occurs at critical shear-offset δ_S when $t_S = t_L$. By equating Eq. (4) and Eq. (6), δ_S can be expressed in terms of sample diameter and testing temperature:

$$\frac{\delta_S}{D} = \frac{(T_L - T)^2}{ZV_o(D - D_c)} \tag{7}$$

Equation (7) can qualitatively describe the observed fractographic changes in shear-localized samples with varying diameter and testing temperature. It predicts increase in δ_S/D with decreasing sample diameter for a fixed temperature, which agrees with the experimental results (Fig. 3a). A smooth fracture surface without vein-pattern is expected at small diameters when the required δ_S for formation of liquid layer exceeds D. The t_S becomes increasingly longer with decreasing D (Eq. (4)) because of decrease in elastic energy release rate. As a result, t_S remains longer than t_L for small diameters and the condition for liquid instability ($t_S = t_L$) is never satisfied while the MSB slides through the entire sample. We observed smooth fracture surface for sample diameters in the range of 500 nm to 2 μ m at room temperature (Fig. 2).

Equation (7) can also explain the effect of testing temperature on the fracture morphology of shear-localized samples. As shown in Fig. 4a, lowering the testing temperature increases δ_S/D that is correctly predicted by the model. According to Eq. (7), the transition from vein-pattern to smooth fracture surface ($\delta_S/D=1$) should occur at larger diameters with decreasing testing temperature. Experimental results show that the transition shifts from ~400 nm at 433 K to 3 µm at 200 K (Fig. 4a). To further check the validity of Eq. (7), we replot the shear-localized δ_S/D data for different temperatures as a function of parameter $(D-D_C)/(T_I-T)^2$. The rescaled data for different temperatures

collapse onto theoretical curve reasonably well (Fig. 7). The theoretical curve was generated by fitting y = A/x, where y and x respectively represent δ_S/D and $(D - D_c)/(T_L - T)^2$, and A is a fitting constant. The rescaling does not consider the temperature dependence of shear band velocity and other material properties, which can explain the remaining scatter in the data. Nonetheless, the model correctly captures the size and temperature equivalence in tensile fracture of MGs in the shear-localized regime.

The critical shear-offset δ_S can also be calculated by rearranging Eq. (7). It predicts decrease in δ_S with increasing temperature and weak diameter dependence. Our experimental data agrees with these predictions except deviation at smaller diameters. It should be noted that the derivation of Eq. (7) assumes that the liquid instability sets in at the same temperature for all diameters. This assumption may not be strictly valid because the morphology of veins varies with sample size suggesting the change in viscosity of liquid layer. Therefore, Eq. (7) should be further refined for quantitative analysis of fracture morphology in MGs. Nonetheless, the ability of Eq. (7) to describe experimental findings clearly indicates the existence of size-temperature equivalence in fracture of MGs in the shear-localized regime.

The similarity between the sample size and the temperature continues in the necked samples. For example, either the reduction in sample diameter from 500 nm to 400 nm at 298 K or lowering the testing temperature to 200 K can prevent the localized failure (Fig. 4a). The neck length shows the same trend with varying sample diameter (Fig. 3b) and testing temperature (Fig. 5). These observations suggest that the origin of size-temperature equivalence in tensile deformation of MGs should be the same for the entire length scale. The liquid layer analysis presented above can explain the size and temperature correlation in the microscale samples where an MSB is visible. Next, we analyze the deformation behavior of nanoscale samples in which formation of an MSB is suppressed.

There are three different hypotheses used to explain the ESB to MSB transition: (1) strain-rate mismatch, (2) energy-based approach, and (3) heating-assisted nucleation of MSB. We analyze the experimental data in the context of these three hypotheses to understand the mechanism of necking in nanoscale MGs. The strain-rate mismatch between an ESB and the surrounding glass increases with applied strain and diverges to infinity when a bonafide MSB is considered to have nucleated. One can think of a critical strain-rate mismatch requirement for an ESB to

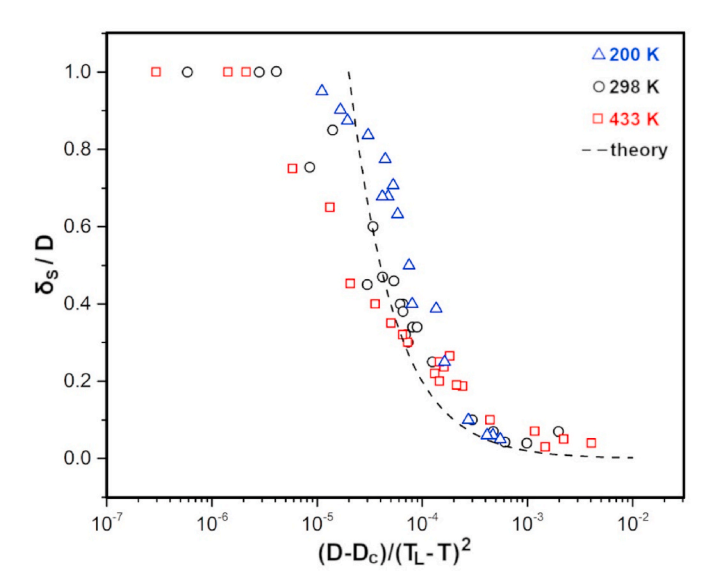


Fig. 7. Rescaling of the fractographic data. The δ_S/D values for shear-localized samples plotted as a function of new variable $(D - D_c)/(T_L - T)^2$. The data for different temperatures collapse onto a single theoretical curve generated by fitting Eq. (7).

transform into an MSB. Schuh et al. derived an expression for the temperature dependence of strain-rate mismatch based on the STZ dynamics [33]:

$$\dot{\Gamma} \propto exp\left(\frac{\phi \cdot \Delta F_0}{kT}\right) \tag{8}$$

where $\dot{\Gamma}$ is the ratio of the strain-rate in the shear band nucleus and the surrounding matrix, ϕ is the fraction of strain energy stored in STZ-sized volume, ΔF_0 is the Helmholtz free energy to operate an STZ, and k is the Boltzmann constant. An ESB can be considered as a nucleus from which an MSB evolves with increasing shear strain. According to Eq. (8), strain-rate mismatch is amplified with decreasing temperature, which should facilitate ESB to MSB transition. However, our experimental results show an opposite trend where necking is favored at lower testing temperatures. Therefore, the concept of critical strain-rate mismatch cannot explain the suppression of ESB to MSB transition in nanoscale MGs.

The energy-based approach introduced in the velocity formula (Eq. (3)) predicts that shear band propagation ceases below critical diameter D_c . This is because the shear band propagation increases the overall energy of the system for samples with $D \leq D_c$. The crossover between the elastic energy and the shear band energy has been used to justify the departure from shear banding in nanoscale MGs [14,21]. While the energy criterion can explain the effect of sample size, it does not correctly describe the size and temperature equivalence observed in present work. Based on Eq. (3) and by considering the temperature dependence of shear band velocity, D_c should increase at higher temperatures which is in contradiction with our experimental findings. Thus, the energy-based approach alone is not sufficient to understand the size and temperature effects in fracture of MGs.

Shimizu et al. proposed heating-assisted transition from ESB to MSB in their ARGL (Aged-Rejuvenation-Glue-Liquid) model of a shear band [57]. The model assumed a progressive shear front moving at velocity of shear wave ($\sim 10^3$ m/s). The validity of ARGL model is justified only for stage I of shear band formation because the experiments have shown synchronized sliding at much lower velocity in stage II. Based on the ARGL description of shear band, a critical length (l_c) of an ESB for formation of an MSB was calculated as [58]:

$$l_{c} = \frac{\alpha C_{v}^{2} \left(T_{g} - T\right)^{2}}{\tau_{glue}^{2} \dot{\delta}} \tag{9}$$

where α is the MG's thermal diffusivity, C_v is its volumetric specific heat, τ_{glue} is the shear strength of glue region in ESB, and $\dot{\delta}$ is the velocity of shear front. According to ARGL model, the key requirement for an ESB to become MSB is that its trailing edge should heat above T_g . This condition can be satisfied only if the length of ESB is equal or greater than l_c . While the heating-assisted nucleation of MSB has been criticized, it can explain the size and temperature effects on the necking transition. If the sample diameter becomes smaller than about l_c , an ESB will not mature due to lack of heat content. Such sample will continue to deform through finely spaced ESBs giving rise to homogeneous-like necking behavior. A decrease in testing temperature increases the l_c , and therefore, the necking transition will shift to larger diameters. The prediction agrees with the experimental findings for three testing temperatures (Fig. 4). The critical diameter D_c increases with decreasing testing temperature.

Based on the properties of Zr-based MG, Shimizu et al. suggested that l_c can vary from few nanometers to micron depending on the velocity of shear front [57]. Such projection was never realized experimentally until the recent work of Tonnies et al. who showed strong loading-rate effect on the critical diameter for localized to homogeneous-like deformation in MGs [32]. Even micron-sized samples can exhibit homogeneous-like flow at low loading rate. Furthermore, it is worth noting that Eq. (9) of ARGL model and Eq. (7) for liquid layer development are essentially the same except the different reference temperatures and shear band velocity values. Therefore, a single heating

assisted mechanism can explain the size and temperature equivalence in the shear-localized and necking regimes during tensile loading of MG.

More insight about size-temperature equivalence in tensile deformation of MGs can be gained from the analogy with the bending studies. It has been shown that bending plasticity increases with decreasing sample thickness and temperature due to increase in number of short shear bands [59,60]. The homogeneous-like flow in nanoscale tensile specimens well below T_g also follows the same size and temperature dependence. Therefore, it is reasonable to hypothesize that the widely reported necking in nanoscale MGs likely stems from the proliferation of embryonic shear bands rather than from true homogeneous flow.

5. Conclusions

The effects of sample-size and testing temperature on the tensile deformation of Pt-Cu-Ni-P metallic glass were quantified using fractographic analysis. We find that the propensity for shear localization and catastrophic failure decreases with reduction in sample diameter and testing temperature below glass transition. The existence of sizetemperature equality in fracture over the entire length scale indicates that the heat generated during plastic deformation is critical in shear band development. The transition from embryonic to mature shear band can be suppressed due to lack of heat content resulting in homogeneouslike necking in nanoscale metallic glasses. Once a major shear band nucleates, the size-temperature equivalence is manifested in the fracture morphology which encompasses varying fractions of vein-pattern and featureless regions. An empirical law based on the heat generated due to shearing and the thermal diffusion can describe the fractographic variations and the size-dependent transition from brittle to ductile behavior of metallic glasses under tension.

Data availability

The raw/processed data required to reproduce these findings cannot be shared at this time as the data also forms part of an ongoing study.

CRediT authorship contribution statement

Chandra Sekhar Meduri: Data curation, Formal analysis, Writing original draft, Experimentation, Data Analysis, Draft Preparation. Jerzy Blawzdziewicz: Data curation, Formal analysis, Data analysis, mathematical model. Golden Kumar: Project administration, Supervision, Writing - review & editing, Writing - original draft, Final Writing and Revision of Manuscript.

Declaration of competing interest

The authors declare that they have no known competing financial interests or personal relationships that could have appeared to influence the work reported in this paper.

Acknowledgements

The work was supported by the National Science Foundation (NSF) through CMMI Award#1919445 and NSF-CAREER Award#1921435.

References

- [1] F. Spaepen, A microscopic mechanism for steady state inhomogeneous flow in metallic glasses, Acta Metall. 25 (1977) 407–415.
- [2] A.S. Argon, Plastic-deformation in metallic glasses, Acta Metall. 27 (1979) 47–58.
- [3] C.A. Schuh, T.C. Hufnagel, U. Ramamurty, Overview No.144 mechanical behavior of amorphous alloys, Acta Mater. 55 (2007) 4067–4109.
- [4] A.L. Greer, Y.Q. Cheng, E. Ma, Shear bands in metallic glasses, Math. Sci. Eng. R 74 (2013) 71–132.
- [5] T.C. Hufnagel, C.A. Schuh, M.L. Falk, Deformation of metallic glasses: recent developments in theory, simulations, and experiments, Acta Mater. 109 (2016) 375–393.

- [6] C.A. Pampillo, H.S. Chen, Comprehensive plastic-deformation of a bulk metallic glass, Mater. Sci. Eng. 13 (1974) 181–188.
- [7] X.J. Gu, S.J. Poon, G.J. Shiflet, J.J. Lewandowski, Compressive plasticity and toughness of a Ti-based bulk metallic glass, Acta Mater. 58 (2010) 1708–1720.
- [8] Z.F. Zhang, J. Eckert, L. Schultz, Difference in compressive and tensile fracture mechanisms of Zr₅₉Cu₂₀Al₁₀Ni₈Ti₃ bulk metallic glass, Acta Mater. 51 (2003) 1167–1179
- [9] T. Mukai, T.G. Nieh, Y. Kawamura, A. Inoue, K. Higashi, Dynamic response of a Pd₄₀Ni₄₀P₂₀ bulk metallic glass in tension, Scripta Mater. 46 (2002) 43–47.
- [10] B.A. Sun, W.H. Wang, The fracture of bulk metallic glasses, Prog. Mater. Sci. 74 (2015) 211–307.
- [11] H. Guo, P.F. Yan, Y.B. Wang, J. Tan, Z.F. Zhang, M.L. Sui, E. Ma, Tensile ductility and necking of metallic glass, Nat. Mater. 6 (2007) 735–739.
- [12] Q.S. Deng, Y.Q. Cheng, Y.H. Yue, L. Zhang, Z. Zhang, X.D. Han, E. Ma, Uniform tensile elongation in framed submicron metallic glass specimen in the limit of suppressed shear banding, Acta Mater. 59 (2011) 6511–6518.
- [13] J. Yi, W.H. Wang, J.J. Lewandowski, Sample size and preparation effects on the tensile ductility of Pd-based metallic glass nanowires, Acta Mater. 87 (2015) 1–7.
- [14] D.C. Jang, J.R. Greer, Transition from a strong-yet-brittle to a stronger-and-ductile state by size reduction of metallic glasses, Nat. Mater. 9 (2010) 215–219.
- [15] Y.F. Shi, Size-independent shear band formation in amorphous nanowires made from simulated casting, Appl. Phys. Lett. 96 (2010) 121909.
- [16] Q.K. Li, M. Li, Assessing the critical sizes for shear band formation in metallic glasses from molecular dynamics simulation, Appl. Phys. Lett. 91 (2007) 231905.
- [17] D. Sopu, A. Foroughi, M. Stoica, J. Eckert, Brittle-to-Ductile transition in metallic glass nanowires, Nano Lett. 16 (2016) 4467–4471.
- [18] R.T. Qu, S.G. Wang, X.D. Wang, S.J. Wu, Z.F. Zhang, Shear band fracture in metallic glass: sample size effect, Mater. Sci. Eng. 739 (2019) 377–382.
- [19] Y. Yang, C.T. Liu, Size effect on stability of shear-band propagation in bulk metallic glasses: an overview, J. Mater. Sci. 47 (2012) 55–67.
- [20] Z.W. Shan, J. Li, Y.Q. Cheng, A.M. Minor, S.A.S. Asif, O.L. Warren, E. Ma, Plastic flow and failure resistance of metallic glass: insight from in situ compression of nanopillars, Phys. Rev. B 77 (2008) 155419.
- [21] C.A. Volkert, A. Donohue, F. Spaepen, Effect of sample size on deformation in amorphous metals, J. Appl. Phys. 103 (2008), 083539.
- [22] A. Bharathula, S.W. Lee, W.J. Wright, K.M. Flores, Compression testing of metallic glass at small length scales: effects on deformation mode and stability, Acta Mater. 58 (2010) 5789–5796.
- [23] O.V. Kuzmin, Y.T. Pei, C.Q. Chen, J.T.M. De Hosson, Intrinsic and extrinsic size effects in the deformation of metallic glass nanopillars, Acta Mater. 60 (2012) 889–898.
- [24] S.X. Song, J.S.C. Jang, J.C. Huang, T.G. Nieh, Inhomogeneous to homogeneous transition in an Au-based metallic glass and its deformation maps, Intermetallics 18 (2010) 702–709.
- [25] D.C. Jang, C.T. Gross, J.R. Greer, Effects of size on the strength and deformation mechanism in Zr-based metallic glasses, Int. J. Plast. 27 (2011) 858–867.
- [26] A. Dubach, R. Raghavan, J.F. Loffler, J. Michler, U. Ramamurty, Micropillar compression studies on a bulk metallic glass in different structural states, Scripta Mater. 60 (2009) 567–570.
- [27] B.E. Schuster, Q. Wei, T.C. Hufnagel, K.T. Ramesh, Size-independent strength and deformation mode in compression of a Pd-based metallic glass, Acta Mater. 56 (2008) 5091–5100.
- [28] M.C. Liu, J.C. Huang, K.W. Chen, J.F. Lin, W.D. Li, Y.F. Gao, T.G. Nieh, Is the compression of tapered micro- and nanopillar samples a legitimate technique for the identification of deformation mode change in metallic glasses? Scripta Mater. 66 (2012) 817–820.
- [29] O.V. Kuzmin, Y.T. Pei, J.T.M. De Hosson, In situ compression study of taper-free metallic glass nanopillars, Appl. Phys. Lett. 98 (2011) 233104.
- [30] D.J. Magagnosc, R. Ehrbar, G. Kumar, M.R. He, J. Schroers, D.S. Gianola, Tunable tensile ductility in metallic glasses, Sci. Rep. 3 (2013) 1096.
- [31] D.J. Magagnosc, G. Kumar, J. Schroers, P. Felfer, J.M. Cairney, D.S. Gianola, Effect of ion irradiation on tensile ductility, strength and fictive temperature in metallic glass nanowires, Acta Mater. 74 (2014) 165–182.
- [32] D. Tonnies, R. Maass, C.A. Volkert, Room temperature homogeneous ductility of micrometer-sized metallic glass, Adv. Mater. 26 (2014) 5715–5721.
- [33] C.A. Schuh, A.C. Lund, T.G. Nieh, New regime of homogeneous flow in the deformation map of metallic glasses: elevated temperature nanoindentation experiments and mechanistic modeling, Acta Mater. 52 (2004) 5879–5891.
- [34] B. Yang, C.T. Liu, T.G. Nieh, M.L. Morrison, P.K. Liaw, R.A. Buchanan, Localized heating and fracture criterion for bulk metallic glasses, J. Mater. Res. 21 (2006) 915–922.
- [35] W.H. Jiang, F.X. Liu, H.H. Liao, H. Choo, P.K. Liaw, In situ thermographic observations on the compression behavior of a relaxed Zr-based bulk-metallic glass, J. Mater. Res. 22 (2007) 368–373.
- [36] W.H. Jiang, F.X. Liu, H.H. Liao, H. Choo, P.K. Liaw, B.J. Edwards, B. Khomami, Temperature increases caused by shear banding in as-cast and relaxed Zr-based bulk metallic glasses under compression, J. Mater. Res. 23 (2008) 2967–2974.
- [37] J.J. Lewandowski, A.L. Greer, Temperature rise at shear bands in metallic glasses, Nat. Mater. 5 (2006) 15–18.
- [38] Y.Q. Cheng, Z. Han, Y. Li, E. Ma, Cold versus hot shear banding in bulk metallic glass, Phys. Rev. B 80 (2009) 134115.
- [39] R.T. Qu, S.G. Wang, G.J. Li, R.F. Wang, X.D. Wang, S.J. Wu, Z.F. Zhang, Shear band fracture in metallic glass: Hot, Scripta Mater. 162 (2019) 136–140.
- [40] X. Xie, Y.C. Lo, Y. Tong, J. Qiao, G. Wang, S. Ogata, H. Qi, K.A. Dahmen, Y. Gao, P. K. Liaw, Origin of serrated flow in bulk metallic glasses, J. Mech. Phys. Solid. 124 (2019) 634–642.

- [41] D.B. Miracle, A. Concustell, Y. Zhang, A.R. Yavari, A.L. Greer, Shear bands in metallic glasses: size effects on thermal profiles, Acta Mater. 59 (2011) 2831–2840.
- [42] L.C. Zhang, F. Jiang, Y.L. Zhao, J.F. Zhang, L. He, J. Sun, Stable shear of Cu₄₆Zr₄₇Al₇ bulk metallic glass alloy by controlling temperature rise, Mater. Sci. Eng. 527 (2010) 4122–4127.
- [43] L. Liu, M. Hasan, G. Kumar, Metallic glass nanostructures: fabrication, properties, and applications, Nanoscale 6 (2014) 2027–2036.
- [44] M. Hasan, G. Kumar, High-throughput drawing and testing of metallic glass nanostructures, Nanoscale 9 (2017) 3261–3268.
- [45] Z. Hu, C.S. Meduri, J. Blawzdziewicz, G. Kumar, Nanoshaping of glass forming metallic liquids by stretching: evading lithography, Nanotechnology 30 (2018), 075302
- [46] G. Kumar, P. Neibecker, Y.H. Liu, J. Schroers, Critical fictive temperature for plasticity in metallic glasses, Nat. Commun. 4 (2013) 1536.
- [47] A.H. Vormelker, O.L. Vatamanu, L. Kecskes, J.J. Lewandowski, Effects of test temperature and loading conditions on the tensile properties of a Zr-based bulk metallic glass, Metall. Mater. Trans. 39A (2008) 1922–1934.
- [48] R.T. Qu, Z.Q. Liu, G. Wang, Z.F. Zhang, Progressive shear band propagation in metallic glasses under compression, Acta Mater. 91 (2015) 19–33.
- [49] M.Q. Jiang, L.H. Dai, On the origin of shear banding instability in metallic glasses, J. Mech. Phys. Solid. 57 (2009) 1267–1292.
- [50] Y.F. Gao, B. Yang, T.G. Nieh, Thermomechanical instability analysis of inhomogeneous deformation in amorphous alloys, Acta Mater. 55 (2007) 2319–2327.

- [51] R. Maass, D. Klaumunzer, J.F. Loffler, Propagation dynamics of individual shear bands during inhomogeneous flow in a Zr-based bulk metallic glass, Acta Mater. 59 (2011) 3205–3213.
- [52] R. Maass, F. Loffler, Shear-band dynamics in metallic glasses, Adv. Funct. Mater. 25 (2015) 2353–2368.
- [53] W.H. Jiang, G.J. Fan, F.X. Liu, G.Y. Wang, H. Choo, P.K. Liaw, Rate dependence of shear banding and serrated flows in a bulk metallic glass, J. Mater. Res. 21 (2006) 2164–2167.
- [54] W.J. Wright, M.W. Samale, T.C. Hufnagel, M.M. LeBlanc, J.N. Florando, Studies of shear band velocity using spatially and temporally resolved measurements of strain during quasistatic compression of a bulk metallic glass, Acta Mater. 57 (2009) 4639–4648.
- [55] K. Georgarakis, M. Aljerf, Y. Li, A. LeMoulec, F. Charlot, A.R. Yavari, K. Chomokhvostenko, E. Tabachnikova, G.A. Evangelakis, D.B. Miracle, A.L. Greer, Shear band melting and serrated flow in metallic glasses, Appl. Phys. Lett. 93 (2008), 031907.
- [56] T. Cramer, A. Wanner, P. Gumbsch, Energy dissipation and path instabilities in dynamic fracture of silicon single crystals, Phys. Rev. Lett. 85 (2000) 788–791.
- [57] F. Shimizu, S. Ogata, J. Li, Yield point of metallic glass, Acta Mater. 54 (2006) 4293–4298
- [58] F. Shimizu, S. Ogata, J. Li, Theory of shear banding in metallic glasses and molecular dynamics calculations, Mater. Trans. 48 (2007) 2923–2927.
- [59] R.D. Conner, W.L. Johnson, N.E. Paton, W.D. Nix, Shear bands and cracking of metallic glass plates in bending, J. Appl. Phys. 94 (2003) 904–911.
- [60] C. Meduri, M. Hasan, S. Adam, G. Kumar, Effect of temperature on shear bands and bending plasticity of metallic glasses, J. Alloys Compd. 932 (2018) 922–927.